molecular pharmaceutics

articles

Methotrexate Conjugated to Gold Nanoparticles Inhibits Tumor Growth in a Syngeneic Lung Tumor Model

Yu-Hung Chen,[†] Chiau-Yuang Tsai,[†] Pon-Yu Huang,[†] Meng-Ya Chang,[†] Pai-Chiao Cheng,[‡] Chen-Hsi Chou,[§] Dong-Hwang Chen,[||] Chrong-Reen Wang,[⊥] Ai-Li Shiau,*[,#] and Chao-Liang Wu*[,†]

Department of Biochemistry and Molecular Biology, Department of Chemistry, Institute of Clinical Pharmacy, Department of Chemical Engineering, Department of Internal Medicine, and Department of Microbiology and Immunology, National Cheng Kung University, Tainan, Taiwan

Received December 22, 2006; Revised Manuscript Received July 6, 2007; Accepted July 17, 2007

Abstract: Methotrexate (MTX), a stoichiometric inhibitor of dihydrofolate reductase, is a chemotherapeutic agent for treating a variety of neoplasms. Impairment of drug import into cells and increase in drug export from cells may render cells resistant to MTX. MTX, when locally administered in a soluble form, is rapidly absorbed through capillaries into the circulatory system, which may also account for therapeutic failure in patients. To retain MTX within tumor cells for longer duration and alter its pharmacokinetic behavior, we proposed a new formulation of MTX bound to the gold nanoparticle (AuNP) that serves as drug carriers. In this study, we developed the MTX–AuNP conjugate and examined its cytotoxic effect *in vitro* and antitumor effect *in vivo*. Spectroscopic examinations revealed that MTX can be directly bound onto AuNP via the carboxyl group (–COOH) to form the MTX–AuNP complex and kinetically released from the nanoparticles. The accumulation of MTX is faster and higher in tumor cells treated with MTX–AuNP than that treated with free MTX. Notably, MTX–AuNP shows higher cytotoxic effects on several tumor cell lines compared with an equal dose of free MTX. This can be attributed to the "concentrated effect" of MTX–AuNP. Administration of MTX–AuNP suppresses tumor growth in a mouse ascites model of Lewis lung carcinoma (LL2), whereas an equal dose of free MTX had no antitumor effect. In conclusion, these results suggest that by combining nanomaterials with anticancer drugs MTX–AuNP may be more effective than free MTX for cancer treatment.

Keywords: Gold nanoparticle; methotrexate; anticancer drug; drug delivery; lung cancer

Introduction

Delivery of chemotherapeutic agents to target cells is not sufficient to induce cell death. Once a chemotherapeutic drug is released inside the cell, it must retain within the cell at concentrations sufficient to inhibit cell growth and functions. Nanoparticles are attractive drug carriers in view of their high tissue permeability, high colloidal stability, and small size. Drugs can be grafted onto nanoparticles via physical adsorption, ionic bonding, and covalent bonding. Methotrexate (MTX), an analogue of folic acid, disrupts cellular folate metabolism by inhibiting its target enzyme, dihydrofolate reductase (DHFR).[1–3] In addition, polyglutamate forms of MTX also exert inhibitory effect on thymidylate synthase and enzymes in the *de novo* biosynthesis of purines. MTX or MTX polyglutamates have shown promise in treating cancers overexpressing folate receptors on their surfaces.[4–6] MTX has been used as a cytotoxic anticancer drug for

* To whom correspondence should be addressed. Chao-Liang Wu: e-mail wumolbio@mail.ncku.edu.tw; Fax +886-6-2741694; Tel +886-6-2353535 ext 5536. Ai-Li Shiau: e-mail alshiau@mail.ncku.edu.tw; Fax +886-6-2363715; Tel +886-6-2353535 ext 5629.

[†] Department of Biochemistry and Molecular Biology.

[‡] Department of Chemistry.

[§] Institute of Clinical Pharmacy.

[||] Department of Chemical Engineering.

[⊥] Department of Internal Medicine.

[#] Department of Microbiology and Immunology.

10.1021/mp060132k CCC: $37.00
Published on Web 08/21/2007

decades. However, tumor cells may develop resistance to MTX through several mechanisms, including decreased uptake through the reduced folate carrier and the folate receptor as well as increased efflux of MTX. To counteract this phenomenon, we fabricated MTX conjugates consisting of poly(glutamic acid) or poly(ethylene glycol), which retain high intracellular concentrations of MTX. These conjugates have been shown to enhance cytotoxic effect and decrease cell survival.[7,8] Despite the success of these conjugates *in vitro*, there is still no clinical method for detecting the levels of MTX taken up by the target cells, which is relevant to its therapeutic efficacy.

MTX has been conjugated to large microparticles (~20 μm) made of gelatin or polyglutaraldehyde to facilitate its uptake by tumor cells.[9,10] These methods of drug delivery provide sustained and kinetic releases of MTX and improve its therapeutic efficacy. However, the large size of the conjugates may limit their applications only to direct intratumoral administration. Efficient delivery of the drug conjugates via the intravenous route may be hampered by their large size. Therefore, to be effective, the drug carrier must be sufficiently small to perfuse out of the bloodstream, penetrate the vessels, and set foot on the target cell of interest. Recently, MTX was conjugated with iron oxide (Fe_3O_4) via peptide bond as a drug delivery system to study its cytotoxic effect on human breast cancer (MCF-7) and cervical cancer (HeLa) cells.[11,12] MTX-grafted nanoparticles were believed to be taken up into cells to a greater degree by the human folate receptor than free MTX. However, since many biomolecules may influence or change the pathways and efficiency of such drug delivery system *in vivo*, which may be more complicated than in the *in vitro* conditions, evaluation of MTX conjugated to nanoparticles *in vivo* is of importance.

MTX conjugated to human serum albumin (HSA) has been tested for its antitumor activity *in vitro* and *in vivo*.[13] The folate-binding protein (folate receptor) and the albumin-binding proteins are two types of receptors as candidates for MTX–HSA uptake. According to this study, we hypothesized that there are two mechanisms for the uptake of the MTX–conjugated gold nanoparticle (AuNP) into tumor cells. One is the folate-binding protein expressed on the surface of cell membrane, where MTX of the conjugate is the ligand. The other is the interaction of AuNP and cell membrane proteins that facilitate the internalization of conjugated MTX. With increased accumulation of intracellular MTX, growth-inhibitory effects of MTX may be dramatically improved. In this study, we developed a drug–nanoparticle conjugate by grafting MTX to the surface of AuNP. Furthermore, we evaluated the pharmacokinetic properties of MTX–AuNP in cancer cells and examined its cytotoxic activity *in vitro* and antitumor effect *in vivo*.

Experimental Section

Preparation and Characterization of MTX-Conjugated Nanoparticles. AuNP was manufactured from the reduction of chloroauric acid (Au^{+3}, $HAuCl_4$) to neutral gold (Au^0) by sodium citrate. Briefly, water solutions of hydrogen tetrachloroaurate trihydrate and trisodium citrate dihydrate were mixed under heavy boiling, resulting in gold particles with a net negative charge from the citrate ions, which stabilize the particles. By variation of the citrate to

(1) Rosowsky, A.; Galivan, J.; Beardsley, G. P.; Bader, H.; Oconnor, B. M.; Russello, O.; Moroson, B. A.; Deyarman, M. T.; Kerwar, S. S.; Freisheim, J. H. Biochemical and biological studies on 2-desamino-2-methylaminopterin, an antifolate the polyglutamates of which are more potent than the monoglutamate against 3 key enzymes of folate metabolism. *Cancer Res.* **1992**, *52*, 2148–2155.
(2) Gangjee, A.; Devraj, R.; McGuire, J. J.; Kisliuk, R. L.; Queener, S. F.; Barrows, L. R. Classical and nonclassical furo[2,3-d]pyrimidines as novel antifolates - synthesis and biological-activities. *J. Med. Chem.* **1994**, *37*, 1169–1176.
(3) McGuire, J. J. Anticancer antifolates: Current status and future directions. *Curr. Pharm. Des.* **2003**, *9*, 2593–2613.
(4) Masson, E.; Relling, M. V.; Synold, T. W.; Liu, Q.; Schuetz, J. D.; Sandlund, J. T.; Pui, C. H.; Evans, W. E. Accumulation of methotrexate polyglutamates in lymphoblasts is a determinant of antileukemic effects in vivo - A rationale for high-dose methotrexate. *J. Clin. Invest.* **1996**, *97*, 73–80.
(5) Barnes, M. J.; Estlin, E. J.; Taylor, G. A.; Aherne, G. W.; Hardcastle, A.; McGuire, J. J.; Calvete, J. A.; Lunec, J.; Pearson, A. D. J.; Newell, D. R. Impact of polyglutamation on sensitivity to raltitrexed and methotrexate in relation to drug-induced inhibition of de novo thymidylate and purine biosynthesis in CCRF-CEM cell lines. *Clin. Cancer Res.* **1999**, *5*, 2548–2558.
(6) Dervieux, T.; Brenner, T. L.; Hon, Y. Y.; Zhou, Y. M.; Hancock, M. L.; Sandlund, J. T.; Rivera, G. K.; Ribeiro, R. C.; Boyett, J. M.; Pui, C. H.; Relling, M. V.; Evans, W. E. De novo purine synthesis inhibition and antileukemic effects of mercaptopurine alone or in combination with methotrexate in vivo. *Blood* **2002**, *100*, 1240–1247.
(7) Hudecz, F.; Clegg, J. A.; Kajtar, J.; Embleton, M. J.; Pimm, M. V.; Szekerke, M.; Baldwin, R. W. Influence of carrier on biodistribution and invitro cytotoxicity of methotrexate branched polypeptide conjugates. *Bioconjugate Chem.* **1993**, *4*, 25–33.
(8) Pinard, M. F.; Jolivet, J.; Ratnam, M.; Kathmann, I.; Molthoff, C.; Westerhof, R.; Schornagel, J. H.; Jansen, G. Functional aspects of membrane folate receptors in human breast cancer cells with transport related resistance to methotrexate. *Cancer Chemother. Pharmacol.* **1996**, *38*, 281–288.
(9) Narayani, R.; Rao, K. P. Controlled-release of anticancer drug methotrexate from bio-degradable gelatin microspheres. *J. Microencapsulation* **1994**, *11*, 69–77.
(10) Hung, C. T.; McLeod, A. D.; Gupta, P. K. Formulation and characterization of magnetic polyglutaraldehyde nanoparticles as carriers for poly-1-lysine-methotrexate. *Drug Dev. Ind. Pharm.* **1990**, *16*, 509–521.
(11) Kohler, N.; Sun, C.; Wang, J.; Zhang, M. Q. Methotrexate-modified superparamagnetic nanoparticles and their intracellular uptake into human cancer cells. *Langmuir* **2005**, *2*, 8858–8864.
(12) Kohler, N.; Sun, C.; Fichtenholtz, A.; Gunn, J.; Fang, C.; Zhang, M. Q. Methotrexate- immobilized poly(ethylene glycol) magnetic nanoparticles for MR imaging and drug delivery. *Small* **2006**, *2*, 785–792.
(13) Wosikowski, K.; Biedermann, E.; Rattel, B.; Breiter, N.; Jank, P.; Loser, R.; Jansen, G.; Peters, G. J. In vitro and in vivo antitumor activity of methotrexate conjugated to human serum albumin in human cancer cells. *Clin. Cancer Res.* **2003**, *9*, 1917–1926.

$HAuCl_4$ concentration ratio, particles with average sizes ranging from 8 to 80 nm were obtained.[14] MTX–AuNP complexes were prepared as follows: 13 nm colloidal gold solution (500 μL) and MTX (25 mM, 5 μL) were added to 500 μL of sodium phosphate buffer (PB) (20 mM). The solution was then mixed gently and incubated at room temperature overnight. Subsequently, the solution was centrifuged at 12 000 rpm for 20 min for three times and rinsed with 1 mL of 0.1 M NaCl in PB (10 mM) between each centrifugation. Finally, the complexes were redispersed in PB (10 mM) to an appropriate volume for further study.

The sample was dropped on a copper mesh coated with an amorphous carbon film for transmission electron microscopy (TEM, JEOL-TEM-1200-EX, Tokyo, Japan) to obtain the images of pure and MTX-conjugated AuNP. Zeta potential distribution was measured by the particle characterizer (Malvern ZetaSizer Nano ZS, Malvern, UK). Briefly, 600 μL of serial 3-fold dilutions of the samples were loaded into the capillary zeta potential cell for measurement. This instrument also includes the DLS (dynamic laser scattering) function, by which the particle size distribution can be analyzed. Furthermore, 10 μL of 10-fold concentrated AuNP, MTX–AuNP, and DNA–AuNP were mixed with 2 μL of 30% glycerol and subjected to 1% agarose gel electrophoresis at 50 V for 40 min in 1 $\times$ Tris-borate–EDTA (TBE) buffer (90 mM Tris-borate and 2 mM EDTA). Herein, the fabrication of DNA–AuNP followed the method described previously.[15] MTX concentration was determined according to the absorbance at 258 nm for UV–vis spectrometer (Gene Spec III, Naka Instruments, Tokyo, Japan). Serial 2-fold dilutions of MTX ranging from 2.5 to 20 μg/mL were used as the standard. Energy spectra of tritium-labeled MTX ([^{3}H]MTX) before and after being absorbed onto AuNP were measured by liquid scintillation counter (Beckman LS5000, Fullerton, CA) in scintillation cocktail (Sigma-Fluor, Sigma, St. Louis, MO). X-ray photoelectron spectroscopy (XPS) measurements were carried out using a ULVAC-PHI AES-650 spectrometer (ULVAC-PHI Inc., Chigasaki, Japan). A Mg Kα X-ray (1253.6 eV) was used as the light source, and the peak positions were internally referenced to the Au 4f peak at 84.0 eV. The base pressure of the chamber was $\sim 5 \times 10^{-10}$ Torr, and the takeoff angle was 90°.

Determination of MTX Adsorption onto and Release from AuNP. Ten microliters of 20-fold concentrated AuNP was reconstituted in 200 μL of MTX (10 μg/mL) and incubated at room temperature for 20 min to 12 h. The mixtures were then centrifuged to separate unadsorbed MTX from MTX–AuNP conjugates. The amount of adsorbed MTX was calculated from the difference between the initial and the free MTX concentrations. The amount of MTX adsorbed onto AuNP after 12 h incubation was defined as 100% adsorption. The adsorption curve was plotted as nonlinear regression. To determine the release curve, 5 μL of concentrated [^{3}H]MTX (specific activity = 10 Ci/mol) was reconstituted in 100 μL of PB or serum-free, phenol red-free Dulbecco's modified Eagle's medium (DMEM) and incubated at 37 °C for 3–125 h. Released [^{3}H]MTX was separated by centrifugation, and the radioactivity was determined by liquid scintillation counter. The amount of [^{3}H]MTX released from the AuNP by dithiothreitol (DTT, 100 mM) treatment for 1 h was defined as 100% release.

Determination of the Influx and Efflux of MTX–AuNP and MTX in LL2 Cells. Accumulation study was performed according to the method described previously with slight modification.[16] Murine Lewis lung carcinoma (LL2) cells (5×10^4) were cultured in DMEM supplemented with 10% fetal bovine serum (FBS) in 24-well plates at 37 °C for 2 days followed by treatment with 0.1 μM of [^{3}H]MTX–AuNP or [^{3}H]MTX (specific activity = 8 Ci/mmol) for 5 min to 1 h. The cells were then washed twice with ice-cold HBS [20 mmol/L HEPES, 140 mmol/L NaCl, 5 mmol/L KCl, 2 mmol/L $MgCl_2$, and 5 mmol/L glucose (pH 7.4)], dissolved in 0.2 N NaOH, and incubated at 65 °C for 1 h. The amount of accumulated radioactivity was determined, and the cellular uptake is expressed as pmol MTX/10^6 cells. MTX efflux assay was performed as previously described with modifications.[17] LL2 cells (5×10^4) were cultured in DMEM supplemented with 10% FBS in 24-well plates at 37 °C for 2 days followed by treatment with 0.1 μM of [^{3}H]MTX–AuNP or [^{3}H]MTX (specific activity = 8 Ci/mmol) for 2 h. After removal of tritium-containing medium, cells were washed twice with ice-cold HBS, and the growth medium was replaced with serum-free culture medium. The cells were further incubated for 10–60 min. The cells were then washed, dissolved in 0.2 N NaOH, and incubated at 65 °C for 1 h. The amount of accumulated radioactivity in cells was determined, and cellular MTX is expressed as the percentage of initial MTX content.

Assessment of Cytotoxic Effect and Antitumor Efficacy of MTX–AuNP. Cell viability was assessed using the MTT assay. Cancer cell lines used in this study include LL2, ML-1 (mouse hepatocellular carcinoma), MBT-2 (mouse bladder cancer), TSGH 8301 (human bladder cancer), TCC-SUP (human bladder cancer), J82 (human bladder cancer), PC-3 (human prostate cancer), and HeLa (human cervical cancer) cells. These cells (2×10^3 cells) were cultured in 96-well plates overnight. MTX–AuNP, MTX, or AuNP was added at the desired concentrations, and the cells

(14) Frens, G. Controlled nucleation for the regulation of the particle size in monodisperse gold suspensions. *Nature: Phys. Sci.* **1973**, *241*, 20–22.

(15) Storhoff, J. J.; Elghanian, R.; Mucic, R. C.; Mirkin, C. A.; Letsinger, R. L. One-Pot Colorimetric Differentiation of Polynucleotides with Single Base Imperfections Using Gold Nanoparticle Probes. *J. Am. Chem. Soc.* **1998**, *120*, 1959–1964.

(16) Zhao, R. B.; Chattopadhyay, S.; Hanscom, M.; Goldman, I. D. Antifolate resistance in a HeLa cell line associated with impaired transport independent of the reduced folate carrier. *Clin. Cancer Res.* **2004**, *10*, 8735–8742.

(17) Assaraf, Y. G.; Rothem, L.; Hooijberg, J. H.; Stark, M.; Ifergan, I.; Kathmann, I.; Dijkmans, B. A. C.; Peters, G. J.; Jansen, G. Loss of multidrug resistance protein 1 expression and folate efflux activity results in a highly concentrative folate transport in human leukemia cells. *J. Biol. Chem.* **2003**, *278*, 6680–6686.

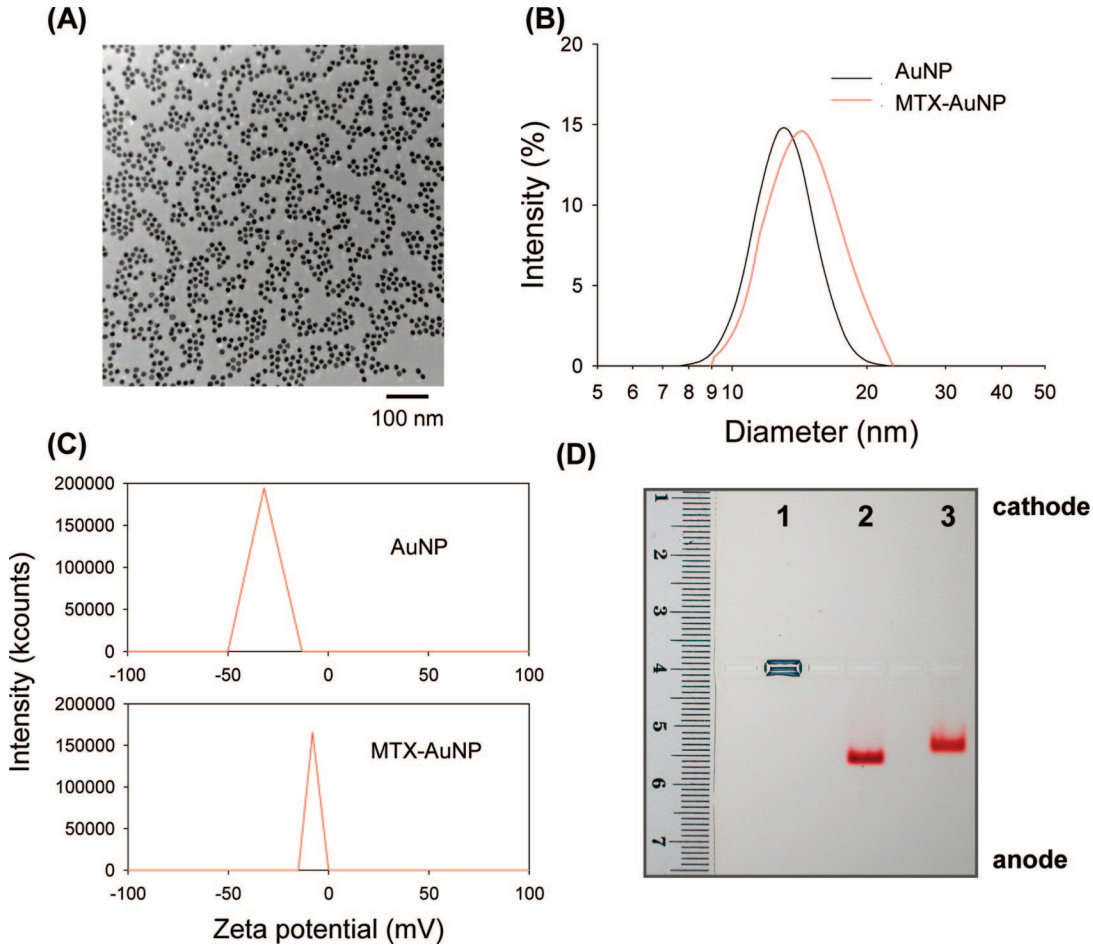

Figure 1. Characterization of MTX–AuNP complexes. (A) The TEM image reveals that MTX–AuNP is monodispersed in PB. The scale bar corresponds to 100 nm. (B) Size distributions of AuNP and MTX–AuNP measured by DLS. (C) Zeta potential measurements of AuNP and MTX–AuNP. The sizes of AuNP and MTX–AuNP are estimated to be 13.2 and 14.3 nm, respectively. (D) Electrophograms of AuNP (lane 1), MTX–AuNP (lane 2), and DNA–AuNP (lane 3) on 1% agarose gel. AuNPs are aggregated in the origin of electrophoresis, whereas MTX–AuNP and DNA–AuNP conjugates migrate toward the anode.

were incubated at 37 °C for 1 h. The medium was then removed and replaced with fresh medium, and the cells were incubated at 37 °C for an additional 71 h. Finally, 40 μL of 1 mg/mL MTT was added to each well, and the plates were incubated at 37 °C for 2 h. Formazan salt crystals were dissolved with 100 μL of DMSO. Absorbance was measured using an enzyme-linked immunosorbent assay (ELISA) reader at the wavelength of 570 nm. For assessing the cytotoxicity of AuNP at a concentration equivalent to the content of AuNP in the AuNP conjugate used for the cytotoxic assay, LL2 cells (5×10^3/well) that had been cultured in 24-well plates overnight were replaced with culture medium in the presence of AuNP (10 nM). The cells were further incubated for 1, 25, and 73 h, and their survival was determined by the MTT assay. The percentage of cell survival is expressed as the mean absorbance of the treated cells divided by the mean absorbance of untreated control cells. The 50% inhibitory concentration (IC_{50}) of the drugs was calculated. For *in vivo* experiments, groups of 5–6 female 8-week-old C57BL/6 mice that had been inoculated intraperitoneally (i.p.) with LL2 cells (5×10^5) at day 0 were treated with 1.8 mg/kg body weight of MTX in the form of MTX–AuNP or MTX in PB or with AuNP or PB alone at days 2, 4, 6, and 8. The mice were sacrificed at day 10, and their ascites and tumors collected and measured. Data are expressed as the mean ± SD, and their statistical differences were assessed by the Student's *t* test.

Results and Discussion

Characterization of MTX–AuNP. The properties of MTX-conjugated AuNP were first determined by TEM, zeta potential measurement, and agarose gel electrophoresis. TEM images reveal that AuNP conjugated with MTX is monodispersed in PB (Figure 1A). From the dynamic light scattering (DLS) measurement, the size of MTX–AuNP is estimated to be 14.3 nm, which is larger than the unmodified 13.2 nm AuNP (Figure 1B). As expected, MTX–AuNP possesses larger hydrodynamic radius. Zeta potential measurements show that surface potential of the unconjugated AuNP is negatively charged with approximately −36.7 ± 15.1 mV, which is attributed to the presence of the protector citrate, a negatively charged molecule, in the synthesis of

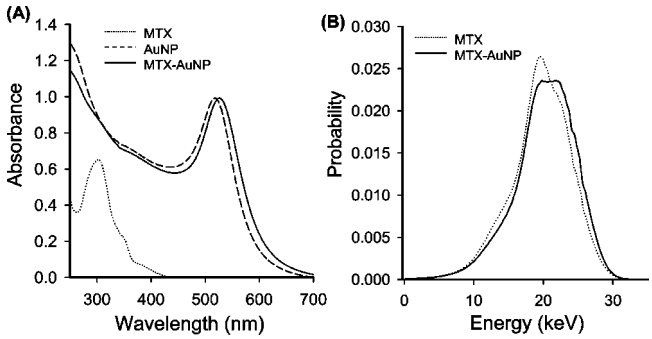

Figure 2. (A) Absorption spectra of MTX, AuNP, and MTX–AuNP. (B) Radio spectra of MTX and MTX–AuNP.

AuNP from the reduction of chloroauric acid by sodium citrate. As MTX molecules are conjugated onto the surface of AuNP, the zeta potential of MTX–AuNP is increased to -7.3 ± 2.5 mV (Figure 1C), indicating the conjugation of MTX molecules onto the surface of AuNP. The sharp-shaped curve of zeta potential distribution reveals not only that the nanoparticle surface is completely conjugated with MTX but also that the nanoparticles exhibit equal sizes in diameter. To further confirm whether the surface of MTX–AuNP possesses a negative charge, agarose gel electrophoresis was used to analyze the mobility of MTX-AuNP (Figure 1D). In the 1 $\times$ TBE running buffer condition, naked AuNP is retained in the origin of electrophoresis and unable to migrate to the anode. This may be due to the fact that under this buffer condition the dielectric layer of naked AuNP protected by citrate is not sufficient to provide a stable system, which results in severe aggregation of AuNP. When MTX molecules are conjugated to AuNP, they can serve as the protector of AuNP and thereby avoid aggregation of AuNP. MTX molecules also provide negative charge for the surface of AuNP and cause migration of AuNP toward the anode, which is similar to the property of DNA-conjugated AuNP.

It is known that AuNP has a prominent surface plasmon band at visible wavelength region. The Au-conjugating suspension that we prepared exhibits absorption at 520 nm (Figure 2A). Furthermore, the peak plasmon absorption is shifted from 520 to 530 nm after MTX adsorption. This 10 nm red shift in the peak plasmon absorption is related to a change in the local dielectric constant around the AuNP as a result of MTX adsorption.[18] Energy spectrum analysis provides the means to study the spectrum of an isotope, a method of particular value for determining the ideal values of window settings for a new isotope. It also provides information to evaluate whether the spectrum is quenched. In Figure 2B, the energy spectrum of [^{3}H]MTX is quenched when it is conjugated onto AuNP in comparison with unconjugated MTX. The observed quenching of energy spectrum may be attributed to the interactions between the MTX molecule and the AuNP. The energy shift is in

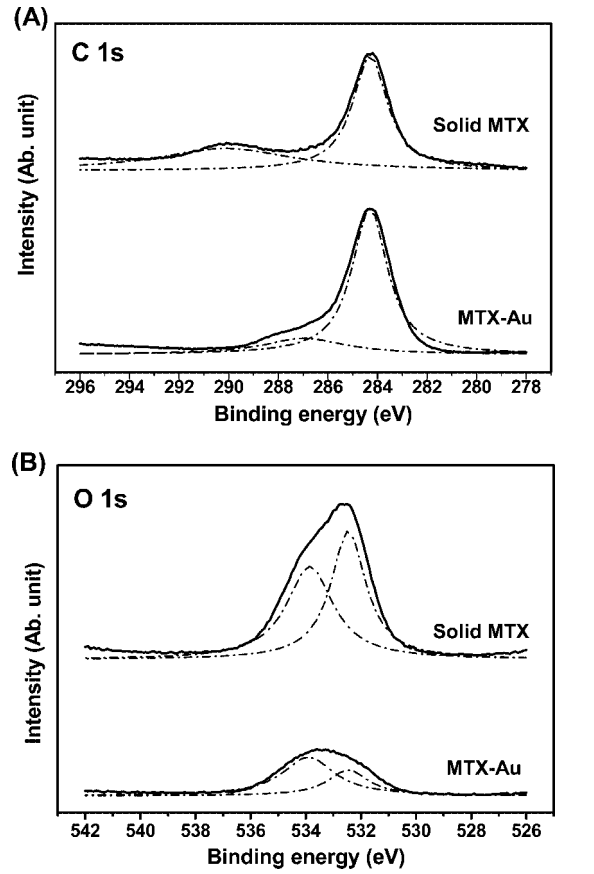

Figure 3. High-resolution XP spectra of C 1s (A) and O 1s (B) photoelectrons of MTX in solid state and in adsorbed state on the AuNP.

agreement with the red shift in the absorption bands of UV–vis spectrum. MTX concentration was measured according to the absorbance at 258 nm. From the intensity of absorption of MTX molecules on the surface of AuNP, the total number of adsorbed MTX and the corresponding surface coverage area per MTX molecule can be calculated. There is 13.1 nmol ($\sim$6.0 μg) of MTX, which is conjugated to 1 mL of 10.78 nM colloidal AuNP, as determined by UV–vis spectroscopy. After calculation, there are 1216 MTX molecules covering one 13 nm AuNP, and the surface coverage area per MTX molecule is $\sim$0.44 nm^2.

To provide further evidence for the chemisorption of MTX on the surface of AuNP, we obtained the XP spectra of MTX in a pure solid form as well as in an adsorbed condition on AuNP. The expected peaks from C 1s and O 1s core levels are clearly detected in all XP spectra. Figure 3 shows the high-resolution XP spectra of solid and adsorbed films of MTX in the C 1s and O 1s spectral regions, respectively. In fact, for solid MTX, two C 1s peaks are identified at 284.5 and 289.6 eV. On the basis of previous studies, these two peaks contribute to the carbon atoms in the aromatic (C–C) and carboxyl (–COOH) moieties, respectively.[19,20] Upon

(18) Cumberland, S. L.; Strouse, G. F. Analysis of the nature of oxyanion adsorption on gold nanomaterial surfaces. *Langmuir* **2002**, *18*, 269–276.

(19) Frydman, E.; Cohen, H.; Maoz, R.; Sagiv, J. Monolayer damage in XPS measurements as evaluated by independent methods. *Langmuir* **1997**, *13*, 5089–5106.

Scheme 1. Model of MTX Conjugated to AuNP Surface

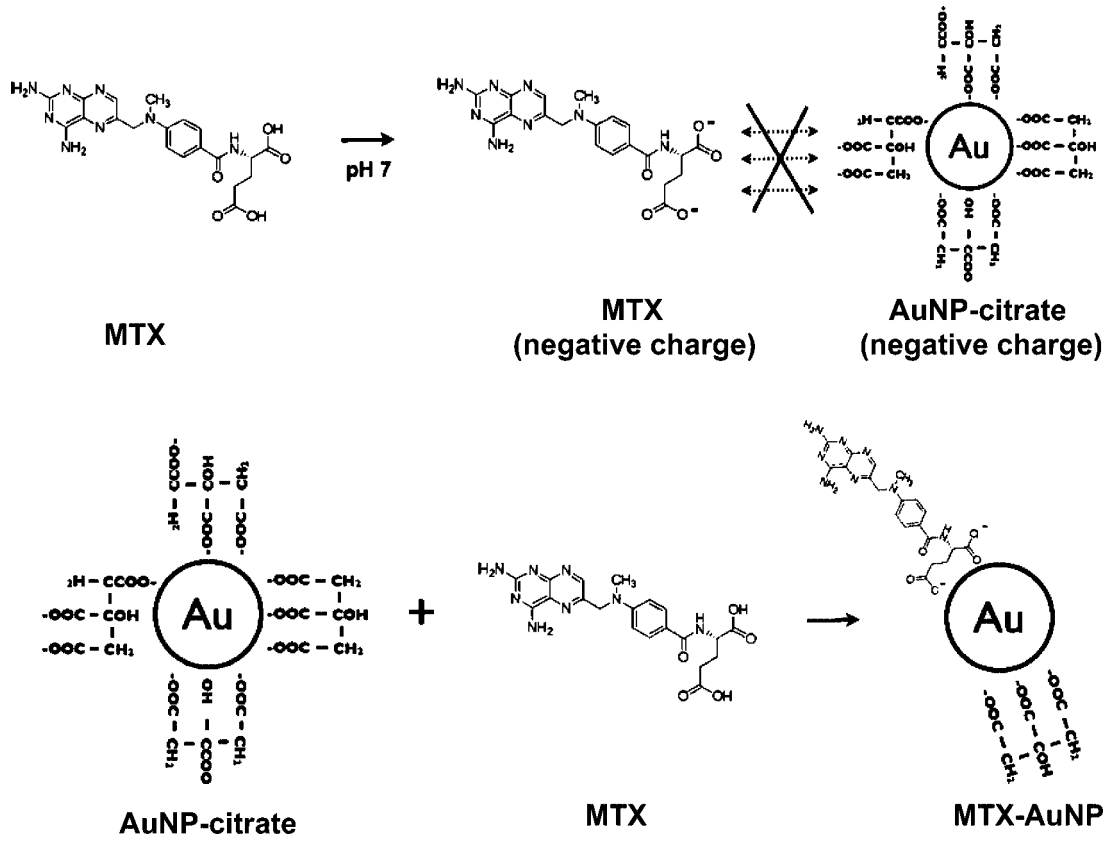

adsorbing on the gold surface, the C 1s peak derived from the carboxylic carbon disappears (289.6 eV). Instead, a peak attributed to the carboxylate (–COO^-) carbon is detected at 289.1 eV. These data provide evidence to indicate that MTX is adsorbed chemically on the gold surface as a carboxylate form. Concerning the O 1s peaks, they are assigned at 531.7 and 533.3 eV for the pure solid MTX using the peak fitting. These two peaks can be attributable to the oxygen atoms in the ring carbonyl (⟩C═O) and the carboxyl (–COOH) moieties, respectively.[19,20] However, for the MTX–AuNP, two peaks (533.2 and 532.4 eV) are fitted using the Microcal Origin 6.0 software (Northampton, MA) (Figure 3B). Given that MTX is adsorbed on the gold surface through the carboxylate group (–COO^-) and that the electron density of oxygen on the carboxylate group is larger than that on the carboxylic group, binding energy of the oxygen on the carboxylate would result in the red shift. Moreover, another peak (533.2 eV) is supposed to arise from the ring carboxyl oxygen (⟩C═O). This implies that, besides the oxygen on carboxylate, the ring carboxyl oxygen of MTX also interacts with the gold surface. All XP spectra were analyzed by peak fitting protocol as described previously.[21]

On the basis of the XPS data and the fact that the carboxylic group is easy to form a coordinate-covalent bond on metal or metal oxide using a localized electron system of COOH, it is conceivable that MTX is conjugated to AuNP through coordinate-covalent bond, leading to a complex formation. The MTX possesses two carboxylic groups (–COOH) and two primary amine groups (–NH_2) shown as Scheme 1. MTX is a weak dicarboxylic acid with pK_a values of 4.8 and 5.5, and its pK_b value of two primary amines is ∼5. From these data, it is reasonable to speculate that MTX is negatively charged at pH 7.4 or under neutral conditions, and its amine groups are not ionized to NH_3^+. AuNP bears a negative charge contributed by the capping molecule citric acid that contains three carboxylic groups. Giving that two negative compounds (AuNP-citrate and MTX) are difficult to close together and form the interaction, and that MTX concentration is much higher than citrate during the formation of the conjugate, it is conceivable that MTX exchanges the citrate on the AuNP surface. The zeta potential measurement reveals that MTX–AuNP exhibits a negative potential, ∼−7.3 eV, and MTX–AuNP is more positive than AuNP, which results from the amine groups with partial positive charge. Furthermore, our results from the XPS analysis also support our proposed model (Scheme 1).

(20) Alexander, M. R.; Payan, S.; Duc, T. M. Interfacial interactions of plasma-polymerized acrylic acid and an oxidized aluminium surface investigated using XPS, FTIR and poly(acrylic acid) as a model compound. *Surf. Interface Anal.* **1998**, *26*, 961–973.

(21) Tosatti, S.; Michel, R.; Textor, M.; Spencer, N. D. Self-assembled monolayers of dodecyl and hydroxy-dodecyl phosphates on both smooth and rough titanium and titanium oxide surfaces. *Langmuir* **2002**, *18*, 3537–3548.

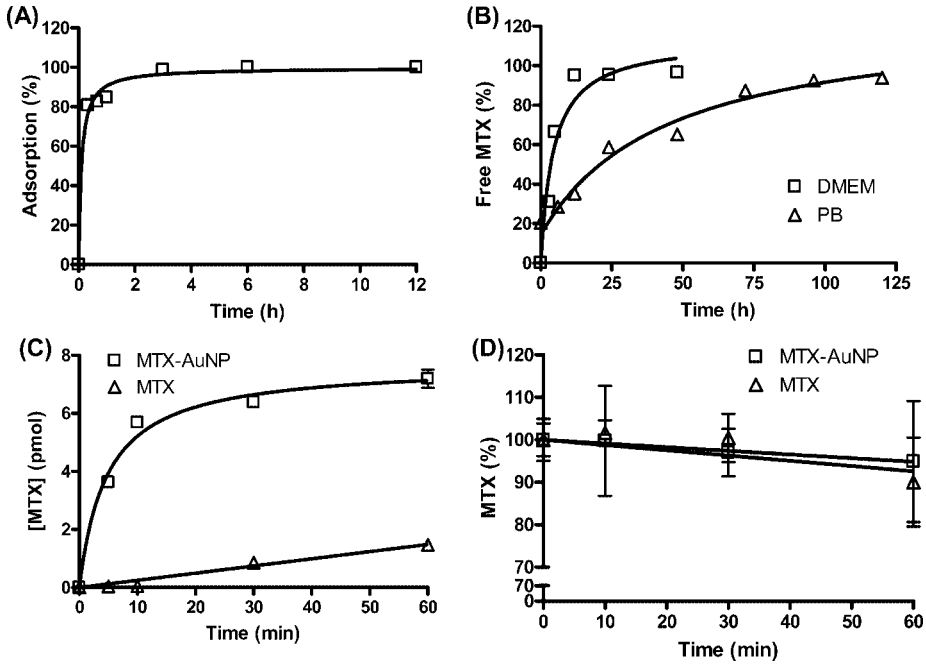

Figure 4. (A) Adsorption curve of MTX onto AuNP. MTX was mixed with AuNP for the indicated times followed by centrifugation to separate unadsorbed MTX from MTX–AuNP conjugates. The amount of adsorbed MTX was calculated from the difference between the initial and the free MTX concentration as determined by spectroscopy. The mount of MTX adsorbed onto AuNP for 12 h incubation is defined as 100% adsorption. (B) Release curve of MTX from the MTX–AuNP conjugate. [^{3}H]MTX–AuNP suspended in PB or serum-free, phenol red-free DMEM was incubated at 37 °C for the indicated times followed by centrifugation to separate free [^{3}H]MTX from the [^{3}H]MTX–AuNP conjugate. The radioactivity of the released [^{3}H]MTX was determined. The amount of [^{3}H]MTX released from the conjugate by DTT treatment for 1 h is defined as 100% release. (C) Influx of MTX–AuNP and MTX in LL2 cells. LL2 cells were treated with 0.1 μM of [^{3}H]MTX–AuNP or [^{3}H]MTX (specific activity = 8 Ci/mmol) for 5 min to 1 h. After wash, the amount of accumulated radioactivity was determined, and the cellular uptake is expressed as pmol MTX/10^6 cells. (D) Efflux of MTX–AuNP and MTX in LL2 cells. LL2 cells were treated with 0.1 μM of [^{3}H]MTX–AuNP or [^{3}H]MTX (specific activity = 8 Ci/mmol) for 2 h and subsequently refed with serum-free DMEM for an additional 10–60 min. After wash, the amount of accumulated radioactivity in cells was determined, and intracellular MTX is expressed as the percentage of initial MTX content (0 min). Each value represents the mean ± SD (n = 3).

MTX Adsorption onto and Release from AuNP. The MTX adsorption curve shown in Figure 4A illustrates that the reaction between MTX and AuNP is rapid and reaches a plateau of adsorption within 3 h, suggesting that the interaction between the carboxylic group of MTX molecule and AuNP is complete in an overnight preparation of MTX–AuNP. The result also suggests that MTX molecules tend to replace citrate and become the protector of AuNP. Next, we evaluated the release kinetics of MTX from MTX–AuNP complexes in the culture medium and PB at 37 °C to mimic biological and nonbiological conditions, respectively. The releasing rate of MTX from MTX–AuNP complexes in culture medium is 9-fold faster than that in PB (Figure 4B). The faster replacement rate in the culture medium may be due to more competitors in the culture medium, such as bovine serum albumin, vitamins, and amino acids, that contain carboxylic or thiol functional group, than in PB. The slopes of linear regression curve in the culture medium and PB are 9.50 and 1.06, respectively, indicating that ~10% of MTX are released into the culture medium per hour when MTX–AuNP complexes are applied to biological experiments. Furthermore, about 90% of MTX is released into the culture medium and PB after 12 and 96 h, respectively. The fact that adsorption rate is faster than releasing rate also implies that the interaction between MTX and AuNP is a stronger force, like coordinate-covalent or/and covalent bond.

Influx and Efflux of MTX–AuNP and MTX in LL2 Cells. The uptakes of MTX–AuNP and MTX were measured in LL2 cells using [^{3}H]MTX. As shown in Figure 4C, [^{3}H]MTX uptake is slow, and only 1.5 pmol of [^{3}H]MTX is accumulated in 10^6 LL2 cells when treated with 0.1 μM [^{3}H]MTX for 60 min. In marked contrast, [^{3}H]MTX–AuNP uptake is very rapid and reaches a plateau after 10 min. Following treatment with 0.1 M [^{3}H]MTX–AuNP for 60 min, 7 pmol of [^{3}H]MTX–AuNP is accumulated in 10^6 LL2 cells. These results demonstrate that MTX–AuNP is accumulated at higher intracellular concentrations after 1 h of incubation compared with MTX. The rapid accumulation of MTX–AuNP also suggests that distinct mechanisms may be involved in the uptake of MTX and MTX–AuNP. We hypothesized that intracellular accumulation of MTX–AuNP takes place through AuNP-mediated endocytosis. However, further studies are needed to elucidate this mechanism.

Having demonstrated a dramatic increase in MTX–AuNP accumulation in LL2 cells, we further investigated the efflux rates of MTX–AuNP and MTX. Notably, effluxes of both [^{3}H]MTX and [^{3}H]MTX–AuNP are slow in LL2 cells, with the mean efflux values of 95% and 90% after 60 min, respectively (Figure 4D). Multidrug resistance proteins and intracellular polyglutamylation are involved in MTX efflux. Since the efflux rates are slow in LL2 cells, most MTX and MTX–AuNP are retained intracellularly. More importantly, AuNP does not affect the properties of MTX efflux.

Cytotoxic Effect of MTX–AuNP on Various Cancer Cells. LL2 cells treated with MTX (1.5 μg/mL) (Figure 5B) or AuNP (10 nM) (Figure 5C) for 1 h reveal no evident morphological changes compared with those treated with culture medium alone (Figure 5A). Furthermore, cell morphology is only slightly changed after treatment with 1.5 μg/mL of MTX–AuNP (Figure 5D). Notably, after 12 h of incubation, AuNP (Figure 5E) and MTX–AuNP (Figure 5F) are uptake by the cells, as revealed by black aggregates. As sizes of MTX–AuNP and free AuNP are less than 15 nm (Figure 1A), which are undetectable under optical microscopy, the observed black dots shown in Figure 5E,F should be AuNP aggregates located intracellularly. In the cytoplasm, since MTX tends to release easily from the MTX–AuNP conjugate by exchange with the thiol-containing compounds, AuNP may form large black aggregates, which can be observed under microscopy. By contrast, either MTX–AuNP or free AuNP is monodispersed in the growth medium supplemented with 10% FBS. Of note, whereas AuNP exhibits negligible effect on cells after 12 h incubation (Figure 5E), MTX–AuNP induces cytotoxic effect (Figure 5F). These observations suggest that AuNP is suitable for the delivery of MTX into cancer cells. From the UV–vis spectroscopy study, there are ~1200 MTX molecules on the surface of one AuNP; in other words, we assumed that one AuNP, with the surface coverage thickness of 1 nm and the volume of $4/3\pi$ ($14^3 - 13^3$) nm^3, is occupied by ~1200 MTX molecules. The local concentration of MTX is equal to 0.3 M. The concentration of MTX conjugated to AuNP is enormously higher (~5 orders) than that of the free MTX in the equal volume, which is ~3 μM. This phenomenon is similar to the well-known "concentrated" in the micelle system.[22] Although without considering the diffusion behavior this calculated prediction value may be overestimated, it is accordant with the trend of our results.

The cytotoxic effects of MTX–AuNP and free MTX on various cancer cells were examined using the MTT assay. Figure 5G shows survival of LL2 cells after 1 h exposure to various concentrations of MTX in the form of either MTX–AuNP or free MTX. MTX–AuNP exerts a higher cytotoxic effect than MTX on LL2 cells at the same dose. LL2 cells are more than 17-fold sensitive to MTX–AuNP compared to free MTX. The values of IC_{50} for MTX–AuNP and free MTX are 0.046 and 0.816 μg/mL, respectively (Table 1). Of note, AuNP at the concentration used for MTX–AuNP does not affect the survival of LL2 cells after exposure to AuNP up to 73 h (Figure 5H). We also tested the IC50 values of MTX–AuNP and free MTX on various

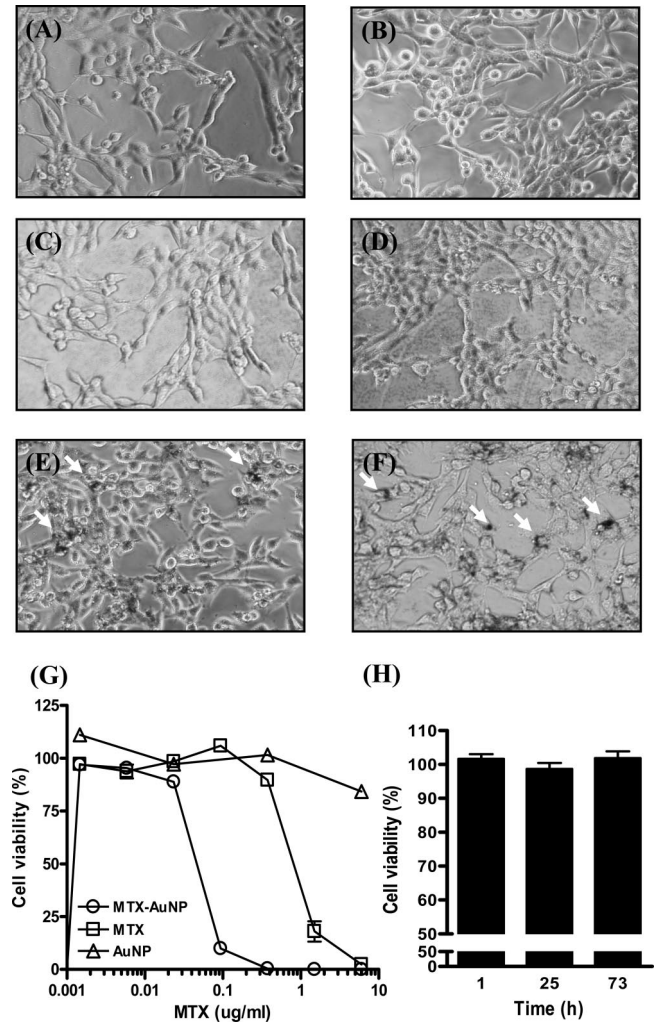

Figure 5. Microscopic images and cell survival of LL2 cells after treatment with MTX, AuNP, or MTX–AuNP. LL2 cells were treated with medium (A), MTX (1.5 μg/mL) (B), AuNP (C), and MTX–AuNP (1.5 μg/mL) (D) for 1 h or with AuNP (E) and MTX–AuNP (F) for 12 h. AuNP uptake by the cells are observed as black dots indicated by white arrows. All micrographs were observed at $\times$200 magnification. (G) Cell survival of LL2 cells after treatment with various concentrations of MTX–AuNP, MTX, or AuNP. LL2 cells treated with various drugs for 1 h were refed with fresh culture medium. Cell survival was determined after 71 h by the MTT assay and expressed as the mean absorbance at 570 nm of the treated cells divided by the mean absorbance of untreated control cells. (H) Cell survival of LL2 cells after treatment with AuNP (10 nM) for 1, 25, and 73 h, as determined by the MTT assay. Each value represents the mean $\pm$ SD ($n = 3$).

(22) Zana, R. Dimeric and oligomeric surfactants. Behavior at interfaces and in aqueous solution: a review. *Adv. Colloid Interface Sci.* **2002**, *97*, 205–253.

Table 1. IC_{50} Values of MTX–AuNP, MTX, and AuNP in Various Cancer Cell Lines

	IC_{50} (μg/mL)[b]			
cell line[a]	MTX–AuNP	MTX	AuNP	sensitivity index[d]
LL2	0.046 ± 0.002	0.816 ± 0.100	N.D.[c]	17.7
ML-1	0.171 ± 0.016	4.228 ± 0.161	N.D.	24.7
MBT-2	0.044 ± 0.003	0.908 ± 0.043	N.D.	20.6
TSGH 8301	0.034 ± 0.003	0.825 ± 0.096	N.D.	24.3
TCC-SUP	0.038 ± 0.006	0.770 ± 0.012	N.D.	20.3
J82	0.136 ± 0.016	1.017 ± 0.159	N.D.	7.5
PC-3	0.132 ± 0.024	0.717 ± 0.002	N.D.	5.4
HeLa	0.052 ± 0.003	0.395 ± 0.139	N.D.	7.6

[a] Cells were exposed to the indicated drug for 1 h, and cell viabilities were determined by MTT assay after a 3 day incubation. [b] IC_{50} values were defined as the drug concentrations at which cell growth was inhibited by 50% compared with drug-free controls. Values are the mean ± SD of three experiments. [c] No measurable cytotoxicity was observed in all the cell lines exposed to AuNP up to the concentration of 300 μg/mL. Therefore, IC_{50} value for each cell line could not be caluclated. N.D. = not detected. [d] Sensitivity index was calculated from IC_{50} of MTX divided by IC_{50} of MTX–AuNP.

human and mouse cancer cell lines. Table 1 shows that all the cell lines tested are more sensitive to MTX–AuNP than to free MTX. Notably, sensitivity indices of some cancer cells, including ML-1, MBT-2, TSGH 8301, and TCC-SUP cells, increase more than 20 times. However, in other cancer cell lines, including J82, PC-3, and HeLa cells, sensitivity indices increase less than 10 times. The cause for the marked difference in the sensitivity index between these two groups of cancer cell lines is not clear, which warrants further studies. To confirm that AuNP has no inherent cytotoxic or growth-inhibitory effects on cells, we determine cell viability in different cancer cells after exposure with various concentrations of AuNP. Our results reveal that AuNP alone has no cytotoxic effect on the cancer cells tested in this study (Table 1). It is of interest to note that high concentrations of AuNP interfere with MTT assay. It is reasonable to speculate that AuNP may interact with MTT crystals or disturb the mitochondrial functions. [^{3}H]-Thymidine incorporation assay may be an alternative method for assessing cell proliferation when this interference occurs.

Antitumor Effect of MTX–AuNP in the LL2 Ascites Tumor Model. We next exploited LL2 cells grown in the peritoneum of syngeneic C57BL/6 mice to test whether MTX and, in particular, MTX–AuNP exerted antitumor effects in terms of reductions of tumor weight and ascites volume. Mice bearing LL2 ascites tumors received three doses of MTX–AuNP, MTX, AuNP, or PB at days 2, 4, 6, and 8. Tumor growth was significantly inhibited in MTX–AuNP-treated mice compared with MTX-treated ($p = 0.0063$) or PB-treated ($p = 0.0106$) mice (Figure 6A). However, the difference in the reduction of tumor growth between MTX–AuNP-treated and AuNP-treated mice was not statistically significant ($p = 0.2617$). Because pleural effusion was a common symptom of lung carcinoma, LL2 ascites tumor model was used to mimic human lung cancer associated with pleural effusion.

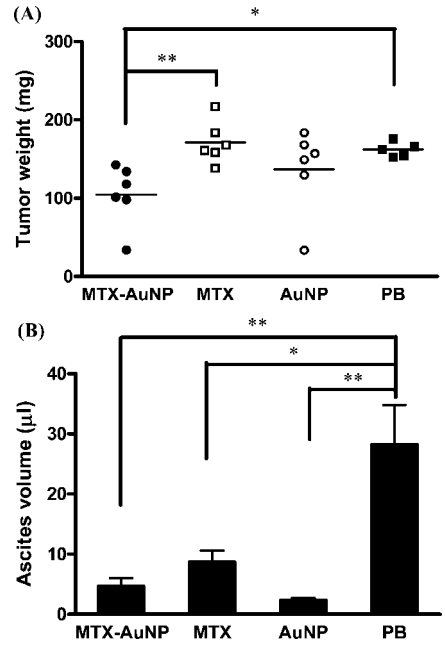

Figure 6. Antitumor effects of MTX–AuNP, MTX, and AuNP in the LL2 ascites tumor model. C57BL/6 mice that had been inoculated i.p. with LL2 cells (5×10^5) at day 0 were treated with 1.8 mg/kg body weight of MTX in the form of MTX–AuNP or MTX in PB or with AuNP or PB alone at days 2, 4, 6, and 8. The mice were sacrificed at day 10, and their tumors and ascites were collected and measured. (A) Individual tumor weights from four groups of mice. Horizontal bars denote the mean value for each group. (B) Ascites volumes from four groups of mice. Data are expressed as the mean ± SD ($n = 5$–6). $^{**}p < 0.01$; $^{*}p < 0.05$ by Student's t test.

As shown in Figure 6B, treatment with MTX–AuNP ($p = 0.0041$), MTX ($p = 0.0132$), or AuNP ($p = 0.0019$) significantly inhibited the formation of ascites compared with PB treatment. However, there was no significant difference in the ascites volume between MTX–AuNP-treated and MTX-treated or AuNP-treated mice. Taken together, these results indicate that MTX–AuNP is more effective than MTX in inhibiting the growth of LL2 ascites tumor. However, MTX–AuNP, MTX, and AuNP are all capable of reducing ascites formation in mice bearing LL2 tumors.

Angiogenesis is a key event during tumor formation and in the pathogenesis of rheumatoid arthritis. Vascular endothelial growth factor (VEGF) plays a crucial role in angiogenesis and vascular permeability. We and others have demonstrated that AuNP can bind to VEGF and further inhibit its angiogenic activity *in vitro* and *in vivo*.[23–25] We recently reported that intraarticular delivery of nanogold is

(23) Mukherjee, P.; Bhattacharya, R.; Wang, P.; Wang, L.; Basu, S.; Nagy, J. A.; Atala, A.; Mukhopadhyay, D.; Soker, S. Antiangiogenic properties of gold nanoparticles. *Clin. Cancer Res.* **2005**, *11*, 3530–3534.

(24) Bhattacharya, R.; Mukherjee, P.; Xiong, Z.; Atala, A.; Soker, S.; Mukhopadhyay, D. Gold nanoparticles inhibit VEGF165-induced proliferation of HUVEC cells. *Nano Lett.* **2004**, *4*, 2479–2481.

an effective treatment strategy for rat collagen-induced arthritis, a model that mimics clinical and histological features of human rheumatoid arthritis.[25] Nanogold exerts antiangiogenic activities and subsequently reduces macrophage infiltration and inflammation, which results in attenuation of arthritis.[25] VEGF, also known as vascular permeability factor, secreted by tumor cells is responsible, in whole or in part, for ascites fluid accumulation during ascites tumor growth.[26] In the present study, we demonstrate that AuNP alone also reduces tumor burden in the peritoneum (Figure 6A) and inhibits ascites formation (Figure 6B) in mice bearing LL2 ascites tumors. Giving the antiangiogenic property of AuNP through its binding to VEGF165 and VEGF121,[25] it is tempting to speculate that such an effect may also contribute to the observed reduction of tumor burden and ascites in LL2 tumor-bearing mice. Since thiolated polyethylene glycol-coated AuNP does not bind to VEGF and hence fail to exert antiangiogenic activity,[25] surface modification of AuNP by MTX is expected to reduce the interaction of AuNP with VEGF. Therefore, regarding the inhibition of ascites formation through binding to VEGF, free AuNP may be more effective than MTX–AuNP. Nevertheless, the antitumor effects of MTX–AuNP are attributed to both MTX and AuNP, which exert a different mode of action.

Conclusions

Because of the great biocompatibility and ease of preparation and characterization, colloidal AuNP has been used in biomedical applications with no known inherent cytotoxicity. Recently, AuNP is widely exploited in biological applications, such as DNA manipulation,[27] plasmid DNA transfection,[28–30] Pb(II) detection,[31,32] and combination in radiotherapy.[33] AuNP functionalized with cationic side chains has been reported to be cytotoxic to Cos-1 monkey kidney cells, resulting from their interactions with the cell membrane, a feature initially mediated by the strong electrostatic attraction to the negatively charged lipid bilayer of cell membrane.[34] In this study, we have included an equal mole of AuNP alone as the control group for assaying cytotoxicity *in vitro* to exclude the possible growth-inhibitory effect of AuNP in the complex of MTX–AuNP.

In conclusion, we successfully synthesized MTX–AuNP and provided an alternative drug formulation of MTX for cancer therapy. Adsorption of MTX molecule on AuNP surface was studied using different analytical techniques. The carboxyl group (–COOH) can strongly bind to AuNP as confirmed by XPS studies. By exploiting AuNP as a drug carrier, MTX is efficiently transported into tumor cells and exerts cytotoxic activity *in vitro* and antitumor effects *in vivo*. Furthermore, our results suggest that MTX–AuNP may have therapeutic potential for cancer treatment.

Acknowledgment. This work was supported by grants from the National Science Council (NSC93-2120-M-006-003 and 94-2120-M-006-001) of Taiwan and the Foundation of Chen, Jieh-Chen Scholarship, Tainan, Taiwan.

MP060132K

(25) Tsai, C. Y.; Shiau, A. L.; Chen, S. Y.; Chen, Y. H.; Cheng, P. C.; Chang, M. Y.; Chen, D. H.; Chou, C. H.; Wang, C. R.; Wu, C. L. Amelioration of collagen-induced arthritis in rats by nanogold. *Arthritis Rheum.* **2007**, *56*, 544–554.

(26) Nagy, J. A.; Masse, E. M.; Herzberg, K. T.; Meyers, M. S.; Yeo, K. T.; Yeo, T. K.; Sioussat, T. M.; Dvorak, H. F. Pathogenesis of ascites tumor growth: vascular permeability factor, vascular hyperpermeability, and ascites fluid accumulation. *Cancer Res.* **1995**, *55*, 360–368.

(27) Mirkin, C. A.; Letsinger, R. L.; Mucic, R. C.; Storhoff, J. J. A DNA-based method for rationally assembling nanoparticles into macroscopic materials. *Nature (London)* **1996**, *382*, 607–609.

(28) Sullivan, M. M. O.; Green, J. J.; Przybycien, T. M. Development of a novel gene delivery scaffold utilizing colloidal gold-polyethylenimine conjugates for DNA condensation. *Gene Ther.* **2003**, *10*, 1882–1890.

(29) Tsai, C. Y.; Shiau, A. L.; Cheng, P. C.; Shieh, D. B.; Chen, D. H.; Chou, C. H.; Yeh, C. S.; Wu, C. L. A biological strategy for fabrication of Au/EGFP nanoparticle conjugates retaining bioactivity. *Nano Lett.* **2004**, *4*, 1209–1212.

(30) Niidome, T.; Nakashima, K.; Takahashi, H.; Niidome, Y. Preparation of primary amine-modified gold nanoparticles and their transfection ability into cultivated cells. *Chem. Commun.* **2004**, 1978–1979.

(31) Liu, J. W.; Lu, Y. A colorimetric lead biosensor using DNAzyme-directed assembly of gold nanoparticles. *J. Am. Chem. Soc.* **2003**, *125*, 6642–6643.

(32) Liu, J. W.; Lu, Y. Accelerated color change of gold nanoparticles assembled by DNAzymes for simple and fast colorimetric Pb^{2+} detection. *J. Am. Chem. Soc.* **2004**, *126*, 12298–12305.

(33) Hainfeld, J. F.; Slatkin, D. N.; Smilowitz, H. M. The use of gold nanoparticles to enhance radiotherapy in mice. *Phys. Med. Biol.* **2004**, *49*, N309–N315.

(34) Goodman, C. M.; McCusker, C. D.; Yilmaz, T.; Rotello, V. M. Toxicity of gold nanoparticles functionalized with cationic and anionic side chains. *Bioconjugate Chem.* **2004**, *15*, 897–900.